Development of a Microwave-Excited Microplasma Thruster

IEPC-2005-056

Presented at the 29th International Electric Propulsion Conference, Princeton University October 31 – November 4, 2005

Yoshinori Takao*, Kouichi Ono†, Kazuo Takahashi‡, and Koji Eriguchi§
Department of Aeronautics and Astronautics, Kyoto University, Kyoto, 606-8501, Japan

This paper proposes a miniature electrothermal thruster using microwave-excited plasmas, which consists of a cylindrical microplasma source and a conical micronozzle. The microplasma source is made of a dielectric tube 10 mm long and 1.5 mm in inner diameter, and the micronozzle is fabricated in a 1.0 mm thick quartz plate with a throat diameter of 0.2 mm. In plasma diagnostics of the microplasma source, high microwave frequency and dielectric constant resulted in desirable plasma characteristics: the electron densities of 10^{16}-10^{19} m^{-3} and the rotational temperatures of 500-1000 K. As a preliminary thrust performance measurement, the thrust and specific impulse obtained were 2.0 mN and 136 s with a thrust efficiency of 12 % at a 4-GHz microwave input power of 5 W and an Ar mass flow rate of 1.5 mg/s.

I. Introduction

MICROSPACECRAFT have recently attracted increasing attention in space technology. The motivation behind this is to reduce the overall mission costs and greatly increase the launch rates. Reducing the scale of spacecraft decreases the launch costs, and simplifying the structure leads to short development periods. In addition, microspacecraft mission scenarios may be envisioned with the mission accomplished by a fleet of several microspacecraft to reduce the mission risk. Such a high reliability as well as low-cost performance is one of the great advantages for microspacecraft, because their repair is not readily done in space.[1]

To realize microspacecraft, their components must be miniaturized drastically, and micropropulsion systems are no exceptions. Various microthrusters have been proposed for microspacecraft applications, being under significant development for primary and attitude control. Such microthrusters require lightweight, small-sized, low-thrust, and small-impulse-bit systems. In practice, however, none of the microthrusters are well established until now, and further research is to be done.

In this paper, we propose a miniature electrothermal thruster using microwave-excited plasmas, which is an application of microplasma sources on which extensive research has recently been done.[2–6] Assuming that plasmas are excited by surface waves, a major feature of such plasmas is that microwaves penetrate into the plasma chamber along the plasma-dielectric interfaces even in the overdense mode and the electron heating occurs in a thin skin-depth layer (a few millimeters deep or less), that is, the power absorption in plasmas becomes maximum at the interfaces.[7–9] Such mechanism of the power deposition is a great advantage to generate plasmas in a very small space without magnetic-field confinement. These features would contribute to a simple structure and long-time operation, compared to other conventional thrusters, because the present thruster requires no electrodes, neutralizers, or magnets. Moreover, the recent development of high-frequency microelectronics devices would also help to realize the microwave-excited microplasma thruster presented here.

*Graduate Student, Department of Aeronautics and Astronautics, Email: yoshinori_takao@kuaero.kyoto-u.ac.jp
†Professor, Department of Aeronautics and Astronautics, Email: ono@kuaero.kyoto-u.ac.jp
‡Research Associate, Department of Aeronautics and Astronautics, Email: takahashi@kuaero.kyoto-u.ac.jp
§Associate Professor, Department of Aeronautics and Astronautics, Email: eriguchi@kuaero.kyoto-u.ac.jp

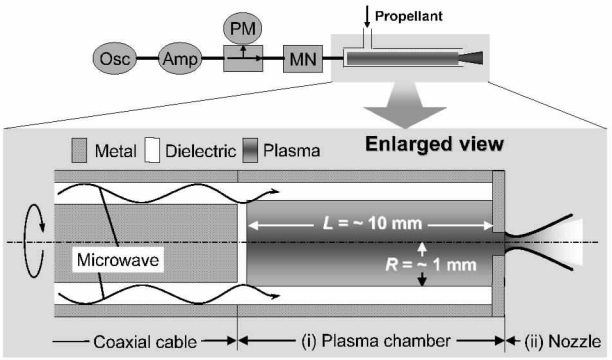

Figure 1. Schematic of the microplasma thruster using microwave-excited plasmas, consisting of an azimuthally symmetric microplasma source and a converging-diverging (Laval) micronozzle. The working gas is Ar in this study.

Figure 1 shows a schematic diagram of the microplasma thruster, which consists of a microplasma source and a micronozzle. The plasma source is composed of a cylindrical dielectric tube, the outside of which is covered with a metal grounded. The inner radius and length of the tube are about 1 and 10 mm, respectively. Microwaves are injected through a coaxial cable into the plasma chamber, where propellant gases are ionized and heated up in the pressure range from 10 kPa to 100 kPa. Such high thermal energy is converted into kinetic energy through the micronozzle to produce the thrust required. On the basis of this concept, we developed a numerical model for design consideration and estimated the thrust performance.[10–12]

The objective of this study is to investigate the plasma characteristics of a microplasma source developed using optical emission spectroscopy (OES) and an electrostatic probe in order to find an optimum operational condition for the microplasma thruster under the condition of microwave input powers below 10 W. First, a microplasma source without a micronozzle was developed to conduct its plasma diagnostics. Then, a micronozzle was also fabricated to evaluate the thrust performance as a preliminarily experimental study. The following sections give some of the results.

II. Experimental

Figure 2 shows a schematic diagram of the experimental setup and a cross-sectional view of the microplasma source. Microwave signals of 2 and 4 GHz generated by an oscillator (Agilent Technologies, 8648D) are amplified through a 4-stage semiconductor amplifier, and then fed through a semi-rigid coaxial cable (RG-405/U) into the plasma chamber made of a straight quartz tube, to generate and sustain the plasma discharges therein. Here, the reflection of microwaves power is suppressed by adjusting the cable length. The quartz tube is connected to the stainless-steel pipe through which a working gas, Ar in this study, is introduced, and is inserted into a stainless-steal chamber evacuated by a dry and turbo-molecular pump. A pressure gauge, equipped with the stainless-steal pipe upstream of the plasma chamber, is used for measurement of the feed gas pressure, which is assumed to be the pressure inside the plasma chamber.

Figure 3 shows an assembly of the microplasma source presently developed. The center conductor of the semi-rigid coaxial cable, protruding 10 mm beyond the insulator and outer conductor, is covered with a ceramic tube; two types of ceramics, mullite (relative permittivity $\varepsilon_d = 6$) and zirconia ($\varepsilon_d = 12$-25), are employed to investigate the dependence on dielectric constants. [Quartz ($\varepsilon_d = 3.8$) tube was partly used as well.] The outer conductor is also covered with a quartz tube for the protection against electrodes erosion. The plasma chamber, made of a quartz tube 10 mm in length and 1.5 mm in inner diameter, has an orifice 0.4 and 0.2 mm in diameter at the exit to vacuum. (In plasma diagnostics, 0.4 mm orifice was mainly employed.) This structure results in a small conductance to keep the pressure inside the plasma chamber much higher than that in the vacuum chamber. The outside of the plasma chamber is covered with a copper grounded which has a single slit for optical diagnostics. Moreover, a copper mesh prevents microwaves from leaking through the slit.

Emission intensities are measured with a spectrometer (Ocean Optics, HR2000CG-UV-NIR) through a quartz optical fiber, the head of which is directly connected to a window of the vacuum chamber without a lens. In the case of precise diagnostics, the emissions are collected by a lens and transmitted to a 25-cm focal

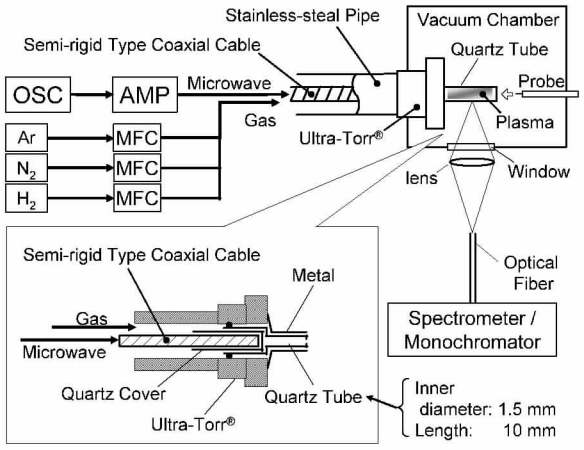

Figure 2. Schematic of the experimental setup and the cross section of the microplasma source developed (bottom).

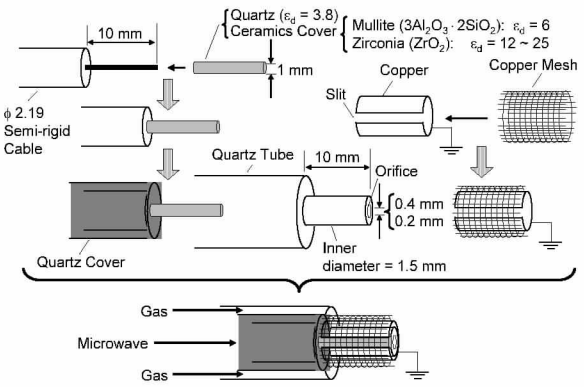

Figure 3. Assembly of the microplasma source presently developed, which has an orifice at the exit to vacuum. The slit of the copper envelope is for optical diagnostics.

length monochromator (Nikon, P250) with a 1200 grooves/mm grating plate. The light emerging from the fiber is focused onto an entrance slit of the monochromator and detected by a photomultiplier (Hamamatsu, R1509). For electrical diagnostics, a cylindrical Langmuir probe, with the probe tip made of a tungsten wire 0.05 mm in diameter and 0.5 mm long, is positioned at an immediate downstream of the orifice to determine the electron density thereat.

III. Plasma Diagnostics

A. Power Dependence of Intensity

Experiments were performed at an Ar flow rate of 50 sccm and a feed gas pressure of 10 kPa. Figure 4 shows photograph images of the emission of microplasma discharges, taken for a total microwave power P_t = (a) 3.5, (b) 5.0, and (c) 7.0 W with a microwave frequency $f = 4$ GHz and mullite tube ($\varepsilon_d = 6$). The plasma was maintained only inside the microplasma chamber at $P_t > 0.3$ W [Fig. 4(a)], the plasma at $P_t > 4$ W was found to flow out into vacuum through the orifice at the end of the plasma chamber, forming a supersonic free jet [Fig. 4(b)], and at $P_t > 6$ W the exhausted plasma was sustained around the end of the plasma source [Fig. 4(c)].

Figure 5 shows the emission intensity (Ar I 763.5 nm) as a function of incident microwave power $P_{in} = P_t - P_{rf}$ for different $f = 2$ and 4 GHz, where P_{rf} is a reflected microwave power, so that P_{in} is assumed to be a net power absorbed in the plasma. Other experimental conditions are the same as in Fig. 4. The emission intensity increases with increasing P_{in}, involving sudden jumps among the regions labeled (a), (b), and (c) in the figure, where these labels correspond to those in Fig. 4. As shown in the figure, higher intensities are observed for the higher microwave frequency at the same incident microwave power; more incident microwave power is required to yield intensity jumps for $f = 2$ GHz.

Figure 6 shows the emission intensity (Ar I 763.5 nm) as a function of incident microwave power P_{in} for different ceramic tubes of $\varepsilon_d = 6$ and 12-25, where other experimental conditions are the same as in Fig. 4. The emission intensity increases with increasing P_{in}, involving sudden jumps among the regions labeled (a), (b), and (c), like the result in Fig. 5. Higher intensities are observed for ε_d = 12-25 at the same incident microwave power. From the results in Figs. 5 and 6, the higher microwave frequency and dielectric constant are found to be desirable to maintain the plasma discharges in the microplasma source developed.

Note that the emission intensities were measured with the spectrometer without light condensing here. The reflected microwave power P_{rf} of 2 GHz could not be suppressed less than 35 % during the emission intensity measurement, whereas that of 4 GHz was kept to be below 10 %. In view of effective use of microwave power, only the microwave frequency of 4 GHz was employed for the rest of experiments discussed below.

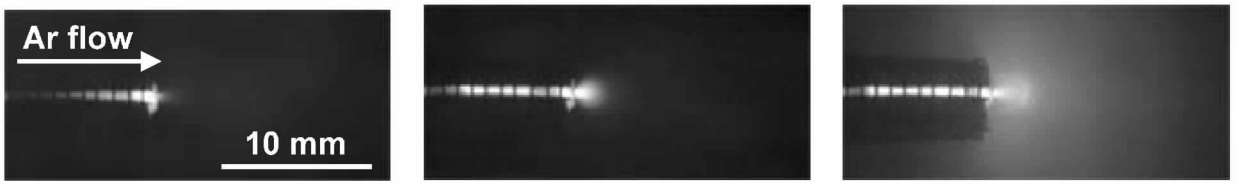

(a) P_t = 3.5 W. (b) P_t = 5.0 W. (c) P_t = 7.0 W.

Figure 4. Photograph images of the emission of microplasma discharges, taken for total microwave power P_t = (a) 3.5, (b) 5.0, and (c) 7.0 W with a microwave frequency f = 4 GHz and mullite tube (ε_d = 6), measured at an Ar flow rate of 50 sccm and a feed gas pressure of 10 kPa.

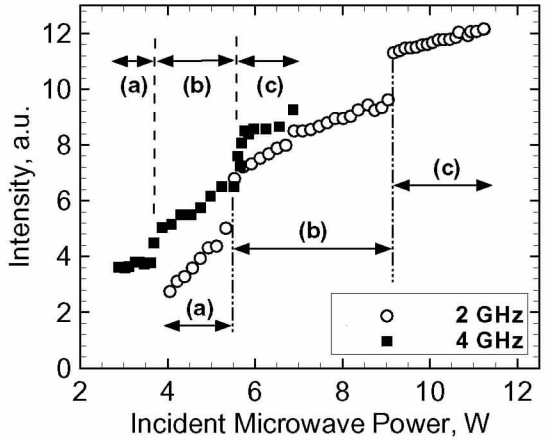

Figure 5. Emission intensity (Ar I 763.5 nm) as a function of incident microwave power $P_{in} = P_t - P_{rf}$ for different microwave frequencies f = 2 and 4 GHz, otherwise measured under the same conditions as in Fig. 4.

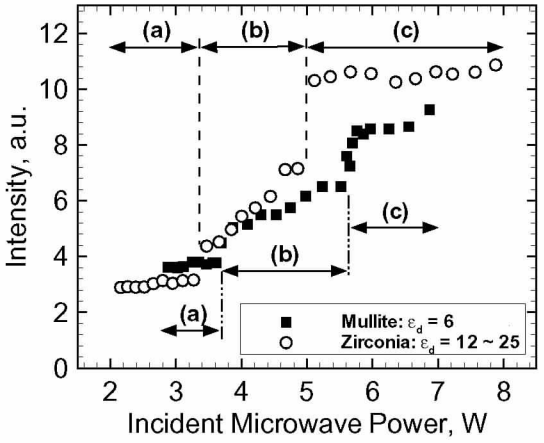

Figure 6. Emission intensity (Ar I 763.5 nm) as a function of incident microwave power $P_{in} = P_t - P_{rf}$ for different dielectric constants ε_d = 6 and 12-25, otherwise measured under the same conditions as in Fig. 4.

B. Electron Density

The results of the intensity measurement imply that high dielectric constants lead to high electron densities in the microplasma source. Figure 7 shows the electron density n_e as a function of incident microwave power P_{in} for different Ar flow rates of 50, 100, 150, 250, and 500 sccm, where corresponding feed gas pressures are 10, 15, 20, 30, and 60 kPa. The electron density increases as P_{in} increases for all Ar flow rates, while decreases with increasing flow rates. High gas flow rates lead to high feed gas pressures in the plasma chamber and affect the plasma discharges; more microwave power is required to sustain high-density plasmas at high flow rates. However, at high incident microwave powers for the zirconia tube, the electron density reaches almost the same values for all mass flow rates, whereas the electron density monotonically decreases with increasing gas flow rates for the mullite one. Note that the Langmuir probe was located at downstream from the orifice as in Fig. 2; thus, the electron density may be larger about an order of magnitude in the microplasma chamber. A critical electron density above which surface waves propagate is about 1.4×10^{18} and 2.6-5.2 $\times 10^{18}$ m^{-3} for the mullite and zirconia tube, respectively, at a microwave frequency of 4 GHz.[7–9] From this fact and experimental results, the plasma was probably sustained by a surface-wave mode at high microwave powers, particularly for the zirconia tube, where the plasma was generated effectively even at high gas flow rates. Moreover, higher electron densities were obtained at the higher dielectric constant as expected.

C. Rotational Temperature

Since the monochromator employed in this paper does not resolve the rotational structure, we have fitted the experimental data with theoretical calculations by using the transition band of N_2 $C^3\Pi_u$-$B^3\Pi_g$ at 380.49 nm

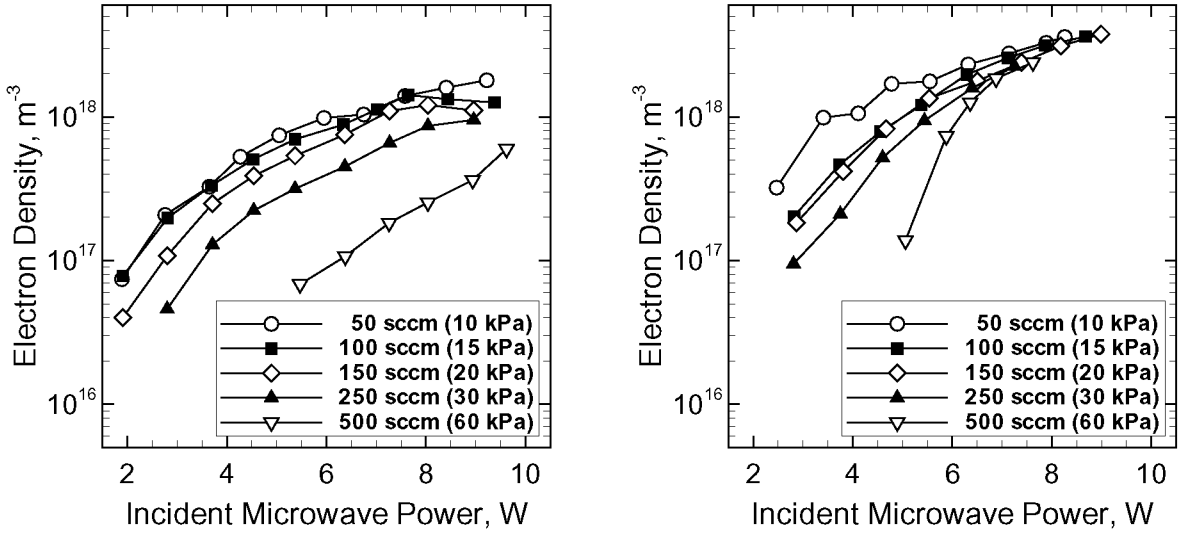

(a) Mullite tube: $\varepsilon_d = 6$. **(b) Zirconia tube: ε_d = 12-25.**

Figure 7. Electron density n_e as a function of incident microwave power P_{in} for different Ar flow rates of 50, 100, 150, 250, and 500 sccm, where corresponding feed gas pressures are 10, 15, 20, 30, and 60 kPa, measured at $f = 4$ GHz. Here, the Langmuir probe was located at an immediate downstream of the orifice as in Fig. 2.

(second positive band),[13,14] in order to calculate the rotational temperature and estimate the gas temperature in the microplasma source.

Figure 8 shows the rotational temperature T_{rot} as a function of position of the plasma discharge for different dielectric constants of $\varepsilon_d = 6$ and 12-25 with photograph images of the emission taken for an incident microwave power $P_{in} = 7$ W, measured at an Ar flow rate of 50 sccm, N_2 flow rate of 0.2 sccm, feed gas pressure of 10 kPa. The rotational temperature increases from upstream to downstream before the exit of the plasma chamber, decreasing at downstream after the orifice. The zirconia tube gives higher rotational temperatures than the mullite one. The wavelength of microwave becomes shorter in a high dielectric constant medium. The photograph images in the figure show a longer discharge area in the mullite-tube-based microplasma source, while a shorter discharge area near the orifice for the zirconia-tube-based one. As Fig. 3 shows, the plasma source has an electrically open end at the orifice, so that the maximum electric field is obtained thereat. The distribution of the rotational temperature showing the maximum temperature at the orifice is consistent with this fact.

Notice that it is important to increase the temperature at the exit of the plasma chamber where a micronozzle will be equipped, because the thermal energy should be effectively converted into the kinetic energy without any undesirable energy loss in the plasma chamber before the micronozzle. Thus, the temperature distribution obtained indicates that the microplasma source is desirable to the miniature thruster presented here.

The discussion above indicates that the high dielectric constant is useful for the microplasma thruster because of the high electron density and rotational temperature in the microplasma source. However, in view of the fact that the long-time operation is required for thrusters of microspacecraft, ceramic tubes have a serious problem; ceramics are vulnerable to a heat shock. In some cases, the ceramic cover used here was found to crack after the long-time plasma diagnostics. To avoid this problem, a quartz tube was employed and we confirmed that it was durable under the long-time operation even at high microwave powers. The following plasma diagnostics and thrust measurement were conducted with a quartz cover.

Figure 9 shows the rotational temperature T_{rot} (N_2) as a function of incident microwave power P_{in} for different orifice diameters $\phi = 0.2$ and 0.4 mm with a microwave frequency $f = 4$ GHz and a quartz tube cover ($\varepsilon_d = 3.8$), together with the electron density. Here, the electron density was measured only at $\phi = 0.4$ mm since less plasma plumes were observed after the orifice at $\phi = 0.2$ mm and no proper voltage-current characteristics were obtained. The lower rotational temperature was obtained at $P_{in} = 7$ W compared to

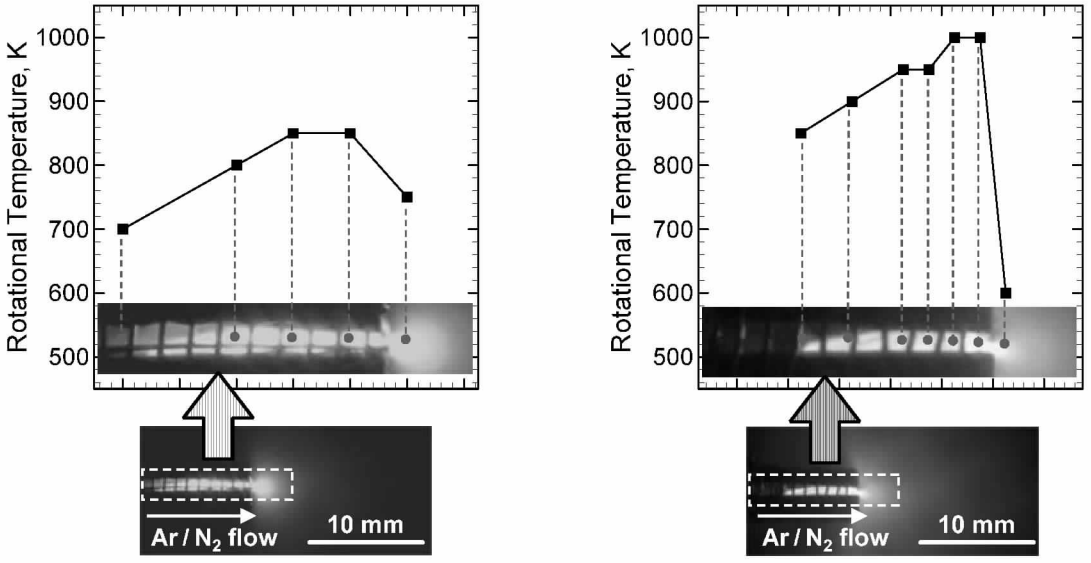

(a) Mullite tube: $\varepsilon_{\rm d} = 6$.

(b) Zirconia tube: $\varepsilon_{\rm d} = 12$-25.

Figure 8. Rotational temperature $T_{\rm rot}$ (N_2) as a function of position of the plasma discharge (top) and photograph images of the emission (bottom), taken for an incident microwave power $P_{\rm in} = 7$ W with a microwave frequency $f = 4$ GHz, measured at an Ar flow rate of 50 sccm, N_2 flow rate of 0.2 sccm, and feed gas pressure of 10 kPa.

that in Fig. 8, because of the low dielectric constant.

The rotational spectra were measured at a fixed feed gas pressure of 10 kPa in Fig. 9(a). The Ar gas flow rates required were 30 and 100 sccm at the orifice diameter $\phi = 0.2$ and 0.4 mm, respectively. The rotational temperature at $\phi = 0.2$ mm is higher than that at $\phi = 0.4$ mm because of the higher microwave power per unit mass flow rate and less cooling effect of the gas flow. The rotational spectra were also measured at a fixed Ar gas flow rate of 50 sccm in Fig. 9(b). The feed gas pressure was 18 and 5 kPa at the orifice diameter $\phi = 0.2$ and 0.4 mm, respectively, and no significant difference of the rotational temperature was observed. Here, the rotational spectra were measured by adding 1 % of nitrogen molecule to Ar gas flows.

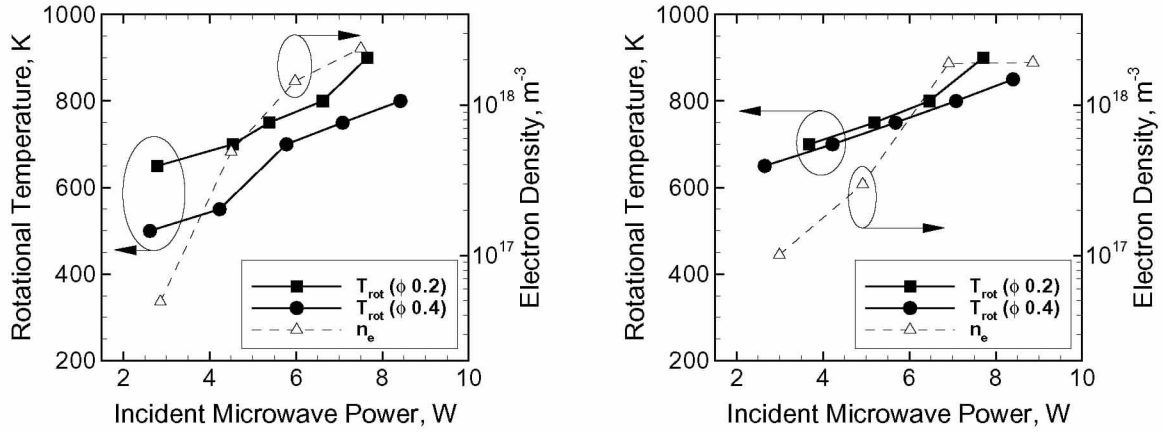

(a) Fixed feed gas pressure: 10 kPa.

(b) Fixed Ar gas flow rate: 50 sccm.

Figure 9. Rotational temperature $T_{\rm rot}$ (N_2) at the orifice as a function of incident microwave power $P_{\rm in}$ for different orifice diameters $\phi = 0.2$ and 0.4 mm with a microwave frequency $f = 4$ GHz and a quartz tube cover ($\varepsilon_{\rm d} = 3.8$), together with the electron density measured at $\phi = 0.4$ mm.

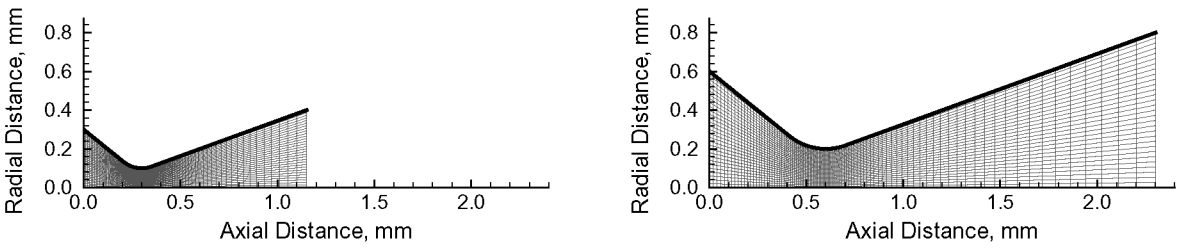

(a) $\phi = 0.2$ mm. (b) $\phi = 0.4$ mm.

Figure 10. Cross-sectional view and computational grid for micronozzles with a 20°-half-cone-angle isothermal wall ($T_{\rm wall} = 300$ K). The radii of the nozzle inlet, throat, and exit are set at 0.3, 0.1, and 0.4 mm, respectively, in (a), while the twice of them in (b). The computational domain of both nozzles is divided into 100 cells in the axial direction and 30 cells in the radial direction.

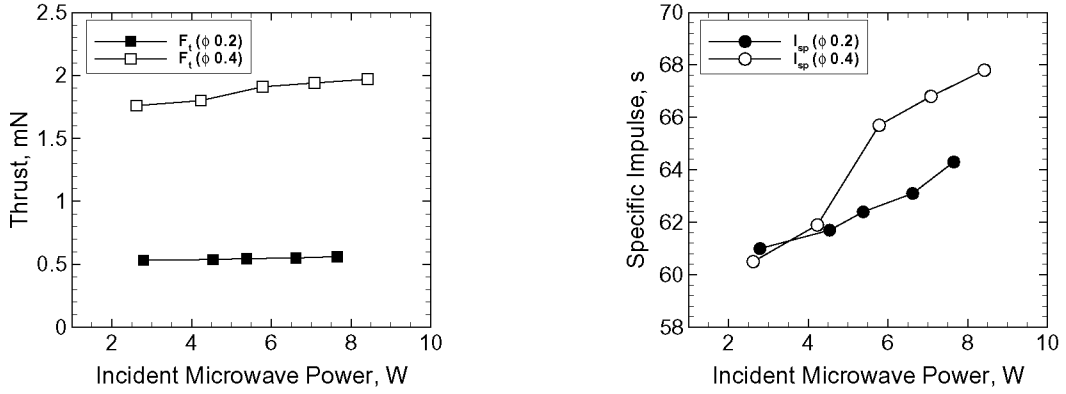

(a) **Thrust** $F_{\rm t}$. (b) **Specific impulse** $I_{\rm sp}$.

Figure 11. Thrust performance as a function of incident microwave power $P_{\rm in}$ for different throat diameters $\phi = 0.2$ and 0.4 mm, calculated at a fixed feed gas pressure of 10 kPa. The nozzle inlet conditions were taken from Fig. 9(a)

IV. Thrust Performance

A. Numerical Analysis

Assuming that the rotational temperature $T_{\rm rot}$ equals the gas temperature $T_{\rm gas}$, we estimated the thrust performance by using the results of plasma diagnostics obtained above and the numerical model developed in Ref. 10–12.

Since the plasma source has an orifice of 0.2 and 0.4 mm in diameter at the exit to vacuum, a micronozzle with a throat 0.2 and 0.4 mm in diameter is assumed to be equipped with the plasma chamber in order to calculate the thrust performance. A cross-sectional view and computational grid for two micronozzles are shown in Fig. 10. As a wall boundary condition, an isothermal wall ($T_{\rm wall} = 300$ K) and non-slip condition were employed.

Figure 11 shows the thrust performance as a function of incident microwave power $P_{\rm in}$ for different throat diameters $\phi = 0.2$ and 0.4 mm, calculated at a fixed feed gas pressure of 10 kPa. Here, the nozzle inlet conditions were taken from Fig. 9(a). The thrust $F_{\rm t}$ at $\phi = 0.4$ mm is more than three times larger than that at $\phi = 0.2$ mm because of the higher gas flow rate. The specific impulse $I_{\rm sp}$ at $\phi = 0.4$ mm is also higher than that at $\phi = 0.2$ mm. Figure 9(a) shows higher rotational temperatures, i.e., gas temperatures at $\phi = 0.2$ mm, so that higher specific impulse was expected. However, a low Reynolds number of 131 at $\phi = 0.2$ mm compared to that of 218 at $\phi = 0.4$ mm resulted in lower specific impulse. At the same gas pressure, small throat diameters and high gas temperatures lead to high viscous loss in the boundary layer of micronozzle.

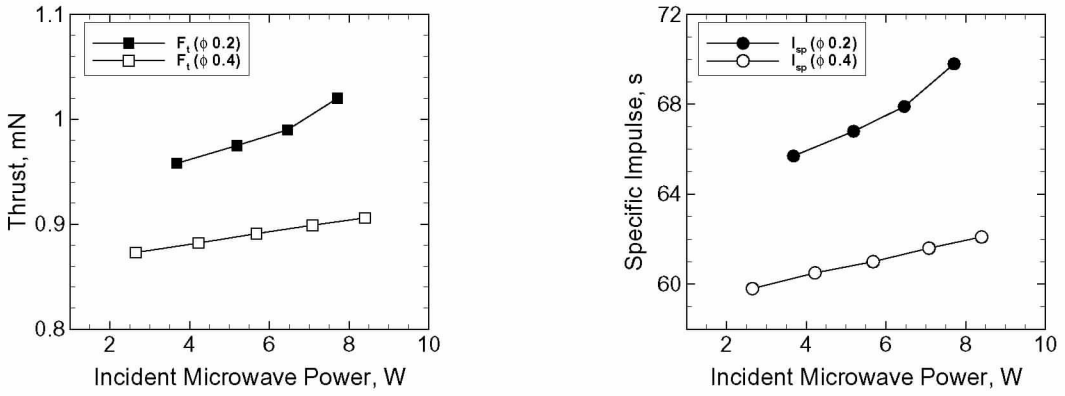

(a) Thrust F_t.

(b) Specific impulse I_{sp}.

Figure 12. Thrust performance as a function of incident microwave power P_{in} for different throat diameters $\phi = 0.2$ and 0.4 mm, calculated at a fixed Ar gas flow rate of 50 sccm (1.5 mg/s). The nozzle inlet conditions were taken from Fig. 9(b)

Figure 12 shows the thrust performance as a function of incident microwave power P_{in} for different throat diameters $\phi = 0.2$ and 0.4 mm, calculated at a fixed Ar gas flow rate of 50 sccm (1.5 mg/s). Here, the nozzle inlet conditions were taken from Fig. 9(b). Both the thrust F_t and specific impulse I_{sp} are higher at $\phi = 0.2$ mm than at $\phi = 0.4$ mm. Figure 9(b) shows almost the same rotational temperature for the two throat diameters, and the feed gas pressure at $\phi = 0.2$ mm is much higher than that at $\phi = 0.4$ mm. This result leads to a high Reynolds number of 219 at $\phi = 0.2$ mm compared to that of 110 at $\phi = 0.4$ mm, so that less viscous loss occurred in the boundary layer of the micronozzle at $\phi = 0.2$ mm. To obtain the high thrust performance, it is desirable to make a throat small and keep high gas temperatures at high gas pressures for a given input microwave power.

B. Measurement of Thrust Performance

As a preliminary experiment, we had a conical micronozzle fabricated in a 1.0 mm thick quartz plate by using conventional machining process with a diamond drill. Figure 13 shows the quartz plate with the micronozzle fabricated, and its cross-sectional and top views taken from an optical microscope. The inlet, throat, and exit diameters are 0.6, 0.2, 0.8 mm, respectively, on the basis of the numerical analysis discussed above. The micronozzle was connected to a straight quartz tube 10 mm long, which was covered with an electrically grounded metal as shown in Fig. 2 except that the metal had no slit. Here, quartz was employed as an microwave antenna cover.

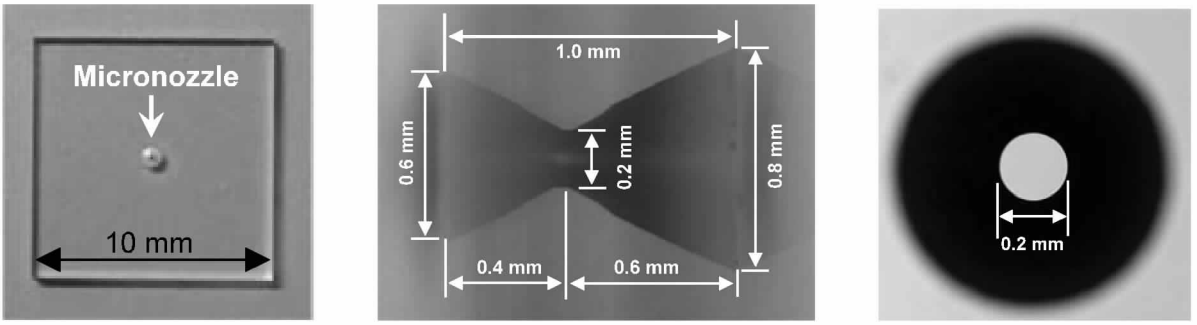

(a) Quartz plate.

(b) Cross-sectional view.

(c) Top view.

Figure 13. Photograph image of a conical micronozzle fabricated in a 1-mm-thick quartz plate, and cross-sectional and top views of the micronozzle

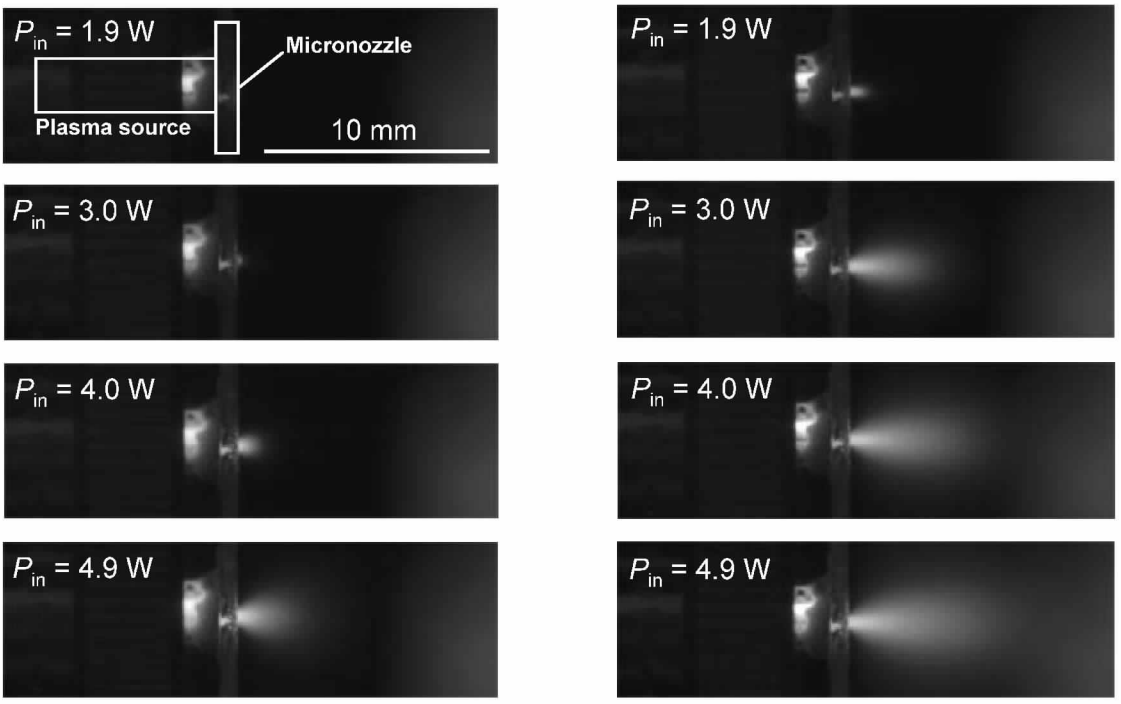

(a) 10 sccm (b) 50 sccm

Figure 14. Photograph images of the thruster operation with the micronozzle shown in Fig. 13 for different Ar gas flow rates of 10 and 50 sccm and for different 4-GHz microwave input powers from 1.9 to 4.9 W.

Figure 14 shows photograph images of the thruster operation for different Ar gas flow rates of 10 and 50 sccm and for different 4-GHz microwave input powers from 1.9 to 4.9 W. The feed gas pressure was 4 and 20 kPa at 10 and 50 sccm gas flow rates, respectively. As microwave power and gas flow rates increase, longer plumes are observed after the micronozzle.

To measure the thrust performance, a small thin ceramic plate was hung downstream of the micronozzle with the thruster fixed tightly, and the displacement of the plate was measured by using a laser displacement gage. This measurement was conducted on both cold-gas and plasma-discharging thruster operation. The relation between displacement and force in cold-gas operation was obtained beforehand by using a pendulum-type thrust stand; this result gives information of the relation of force to mass flow rate of a cold-gas thruster. The thrust was measured by comparing the displacement of the ceramic plate in cold-gas operation and that in plasma-discharging operation. This awkward measurement was conducted because it was impossible to measure the displacement of the thruster by using a pendulum-type thrust stand during the plasma-discharging operation. Microwaves were injected through a semi-rigid and flexible coaxial cable, and the thermal expansion of the cable during the measurement degraded the S/N ratio of the thrust measurement.

Figure 15 shows the thrust performance as a function of Ar gas flow rate at a 4-GHz microwave input power of 5 and 0 W. Here, 0 W means cold-gas operation without plasma discharges. The thrust performance was improved by discharging the plasma, and at an Ar gas flow rate of 50 sccm (1.5 mg/s) the thrust and specific impulse obtained were 2.0 mN and 136 s, respectively, with a thrust efficiency of 12 %. However, the result of the measurement was much better than that estimated by numerically in the preceding section. This discrepancy may result from inaccuracy of the thrust measurement or the numerical model developed. The further thrust measurement and its comparison with numerical estimations are underway.

V. Conclusions

A miniature electrothermal thruster using microwave-excited plasmas has been proposed. The thruster is composed of a cylindrical microplasma source and a conical micronozzle. The microplasma source is made of a dielectric tube 10 mm long and 1.5 mm in diameter, and the micronozzle is fabricated in a 1.0 mm

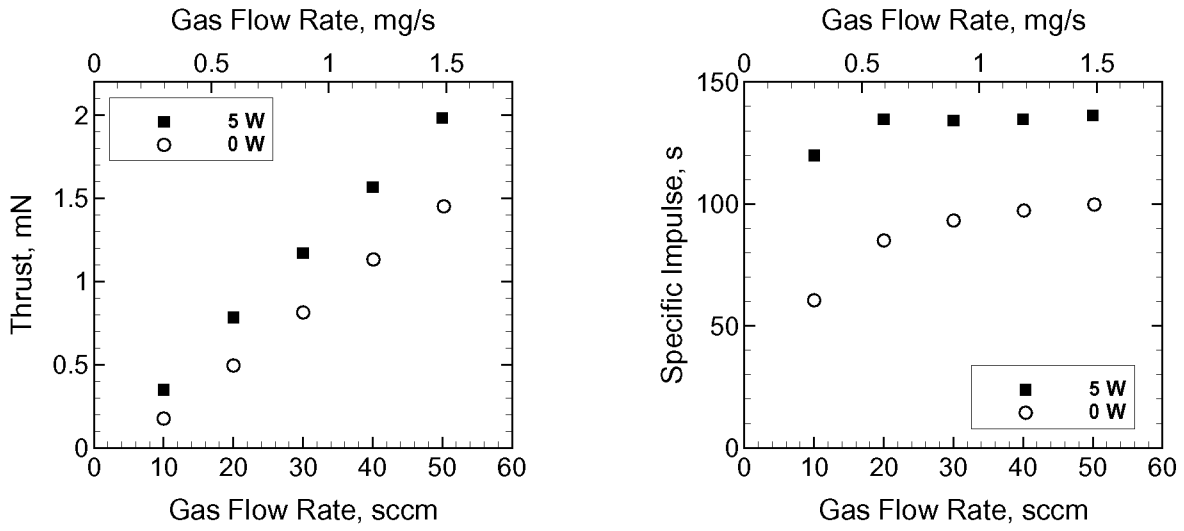

(a) Thrust **(b) Specific Impulse**

Figure 15. Thrust performance as a function of Ar gas flow rate at a 4-GHz microwave input power of 5 and 0 W. Here, 0 W means cold-gas operation without plasma discharges.

thick quartz plate with a throat diameter of 0.2 mm. The microplasma source has been investigated by optical emission spectroscopy and an electrostatic probe. The results of diagnostics show that the emission intensity, electron density, and rotational temperature increase with increasing incident microwave power, microwave frequency, and dielectric constant. The distribution of the rotational temperature inside the microplasma chamber indicates that the microplasma source presented here is desirable to the microthruster, because the temperature increases at the exit of the plasma chamber where a micronozzle is equipped. In the range of microwave powers 2-10 W and of Ar gas flow rates 50-500 sccm, the electron densities and rotational temperatures obtained were 10^{16}-10^{19} m^{-3} and 500-1000 K, respectively. As a preliminary thrust performance measurement, the thrust and specific impulse obtained were 2.0 mN and 136 s with a thrust efficiency of 12 % at a 4-GHz microwave input power of 5 W and an Ar mass flow rate of 1.5 mg/s.

Acknowledgments

This work was supported by a Grant-in-Aid for Scientific Research from the Ministry of Education, Culture, Sports, Science and Technology, Japan. Y. Takao is supported by Research Fellowships of the Japan Society for the Promotion of Science for Young Scientists.

References

[1]Micci, M. M., and Ketsdever, A. D. (ed.), *Micropropulsion for Small Spacecraft*, Progress in Astronautics and Aeronautics Vol.187, American Institute of Aeronautics and Astronautics, Reston, VA, 2000, Chap. 3.

[2]Terashima, K., Howald, L., Haefke, H., and Guntherodt, H., "Development of a Mesoscale/Nanoscale Plasma Generator," *Thin Solid Films*, Vol. 281-282, 1996, pp. 634-636.

[3]Yoshiki, H., and Horiike, Y., "Capacitively Coupled Microplasma Source on a Chip at Atmospheric Pressure," *Jpn. J. Appl. Phys.*, Vol. 40, Part 2, No. 4A, 2001, pp. L360-362.

[4]Hopwood, J., Minayeva, O., and Yin, Y., "Fabrication and Characterization of a Micromachined 5 mm Inductively Coupled Plasma Generator," *J. Vac. Sci. Technol. B*, Vol. 18, No. 5, 2000, pp. 2446-2451.

[5]Bilgic, A. M., Engel, U., Voges, E., Kuckelheim, M., and Broekaert, J. A. C., "A New Low-Power Microwave Plasma Source Using Microstrip Technology for Atomic Emission Spectrometry," *Plasma Sources Sci. Technol.*, Vol. 9, 2000, pp. 1-4.

[6]Iza, F., and Hopwood, J. A., "Low-Power Microwave Plasma Source Based on a Microstrip Split-Ring Resonator," *IEEE Trans. Plasma Sci.*, Vol. 31, No. 4, 2003, pp. 782-787.

[7]Moisan, M., and Zakrzewski, Z., "Plasma Sources Based on the Propagation of Electromagnetic Surface Waves," *J. Phys. D: Appl. Phys.*, Vol. 24, 1991, pp. 1025-1048.

[8]Sugai, H., Ghanashev, I., and Nagatsu, M., "High-Density Flat Plasma Production Based on Surface Waves," *Plasma Sources Sci. Technol.*, Vol. 7, 1998, pp. 192-205.

[9]Ganachev, I., and Sugai, H. "Advanced Large-Area Microwave Plasmas for Materials Processing" *Surf. Coat. Technol.*, Vol. 174-175, 2003, pp. 15-20.

[10]Takao, Y., and Ono, K., "Development and Modeling of a Microwave-Excited Microplasma Thruster," AIAA Paper 2004-3621, 2004.

[11]Takao, Y., Ono, K., Takahashi, K., and Setsuhara, Y., "Microwave-Sustained Miniature Plasmas for an Ultra Small Thruster," *Thin Solid Films*, (to be published).

[12]Takao, Y., and Ono, K., "Miniature Electrothermal Thruster Using Microwave-Excited Plasmas: A Numerical Design Consideration," *Plasma Sources Sci. Technol.*, (unpublished).

[13]Arnold, J. O., Whiting, E. E., and Lyle, G. C., "Line by Line Calculation of Spectra from Diatomic Molecules and Atoms Assuming a Voigt Line Profile," *J. Quant. Spectrosc. Radiant. Transfer.*, Vol. 9, 1969, pp. 775-798.

[14]Phillips, D. M., "Determination of Gas Temperature from Unresolved Bands in the Spectrum from a Nitrogen Discharge," *J. Phys. D: Appl. Phys.*, Vol. 8, 1975, pp. 507-521.